Chapter 3 Theoretical Background

3.1 Introduction

This chapter includes the theoretical background. This chapter deals with the detailed derivation of formulation of the shifting of neutral axis. Finite element formulation for generalized thermoelasticity is also presented in the chapter. Also, Strain Energy Release Rate has been computed under thermo-mechanical loading. It also includes the governing equation of functionally-graded bimodular thermo-elasticity. It also deals with the bimodular property of composites. Calculation of bimodulus ratio and shifting of neutral axis of graphite/epoxy composite has been done through FE based software.

3.2 Basic Theory of bimodularity in composites

3.2.1 Assumptions

Ambartsumyan linearized the nonlinear model, the constitutive relationship between stress and strain as the two linear lines with different slopes, as shown in Figure 3.1 [52].

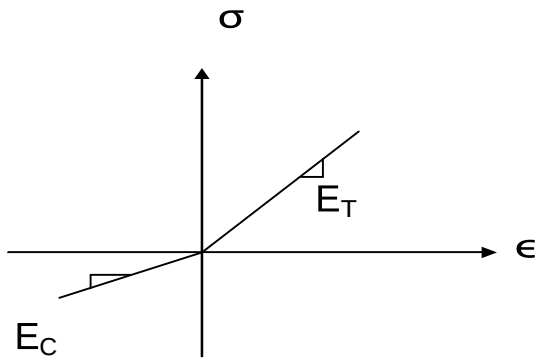

Figure 3.1 Stress-stain curve for bimodular material

The assumptions that are considered for the bimodular beam theory and finite element model are as follows-

1. The material is continuous, homogeneous and anisotropic.
2. There is no shear deformation.
3. It is assumed that straight planes of cross-section of beam before application of the load remain plane after the application of load.
4. The stress- strain relationship is bilinear.

3.2.2 Formulation for equation of deformed shape

The equation of the deformed shaped according to the shape of the deformed uniformly loaded simply supported beam (Figure 3.2) is

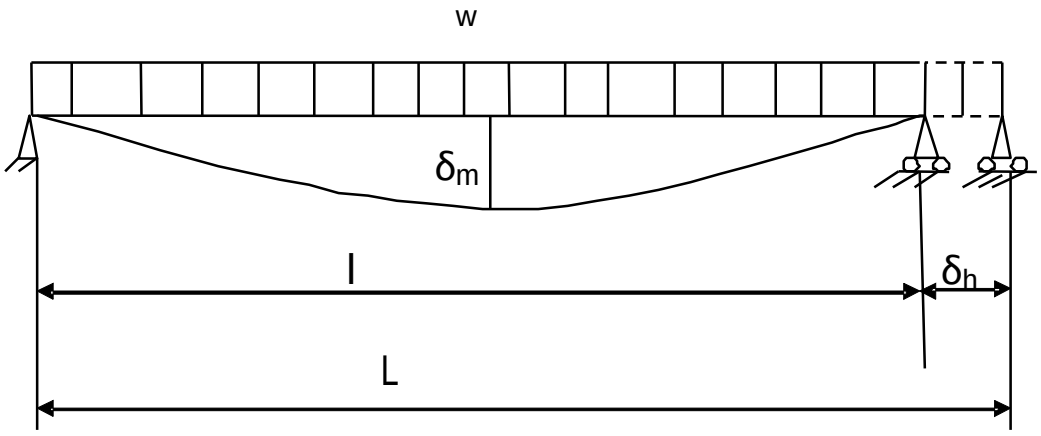

Figure 3.2 Simplysupported uniformly loaded beam

$$\delta_b(x) = D\sin\frac{\pi x}{l} \tag{3.1}$$

where

D : constant

$\delta_b(x)$: deflection of the beam due to bending stress only.

l : length of the projection of the deformed beam on x-axis.

Applying the Boundary Conditions:

$$\delta_b(x=0)=0 \,\&\, M(x=0)=0$$
$$\delta_b(x=l)=0 \,\&\, M(x=l)=0 \tag{3.2}$$

where

$M(x)$: bending moment

Since $\delta_b(x=0)=0$, and $\delta_b(x=l)=0$, these conditions are satisfied and from the symmetry of the deformed shape and the equation, it can be concluded that deflection at the middle of the beam is given as

$$\delta_b(x)=\delta_m$$
$$So, D=\delta_m \tag{3.3}$$
$$\delta_b(x)=\delta_m \sin\frac{\pi x}{l}$$

where,

δ_m: maximum deflection of the beam due to bending.

Equation of bending moment

$$M(x)=EI(\frac{\pi}{l})^2\delta_m \sin\frac{\pi x}{l}(1-\frac{3}{2}(\frac{\pi}{l})^2\delta_m^2\cos^2\frac{\pi x}{l}) \tag{3.4}$$

where

EI : flexural rigidity of the beam

At mid span,

$$M(x=\frac{1}{2})=EI(\frac{\pi}{l})^2\delta_m \tag{3.5}$$

Equation of bending moment in terms of uniformly distributed load:

$$M(x)=\frac{wL}{2}x-\frac{wx^2}{2}\frac{L}{l} \tag{3.6}$$

where

w : uniformly distributed load

L : length of the beam without deformation

So the maximum bending moment will be

$$M(x=\frac{l}{2})=\frac{wLl}{8} \tag{3.7}$$

So the equation of the deformed shape becomes

$$\delta_b(x)=\frac{wLl^3}{8\pi^2 EI}\sin\frac{\pi x}{l} \tag{3.8}$$

3.2.3 Location of neutral axis

It is well known that the neutral axis (N.A.) of the bimodulus beam gets shifted. Evaluation of neutral axis shift, by using the concept of Jadan [51], can be done by assuming the summation of the axial forces on the cross-section of the beam is equal to zero.

Considering the beam section as shown in Figure 3.3 and taking into account the assumptions made,

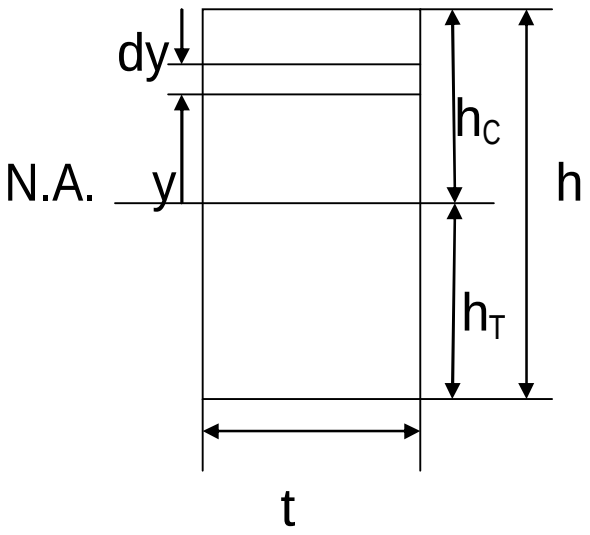

Figure 3.3 A cross-section of a bimodular beam

$$\Sigma F = 0$$

$$\int_{-h_t}^{h_c} \sigma t dy = 0 \tag{3.9}$$

Also,

$$h_T + h_C = h \tag{3.10}$$

where F – sum of axial forces

σ - stress

t – width of the beam

h_C - height of the beam above neutral axis in compression region

h_T - height of the beam below neutral axis in tension region

h – total height of the beam

For bimodulus beam,

$E = E_T$ when $y = h_T$

$E = E_C$ when $y = h_C$ (3.11)

where E_T - modulus of elasticity for tension

E_C - modulus of elasticity for compression

Solving above equations give

$$h_T = \frac{\sqrt{E_C}}{\sqrt{E_C} + \sqrt{E_T}} h \text{ and}$$

$$h_C = \frac{\sqrt{E_T}}{\sqrt{E_C} + \sqrt{E_T}} h \tag{3.12}$$

3.3 Functionally graded bimodular thermo-elasticity and its governing equations

Assuming the symmetry of elastic compliance, $a_{ij} = a_{ji}\ (i, j = 1,2,3)$, for a temperature change of ΔT and coefficient of thermal expansion θ_α, the stress strain relations of bimodulus isotropic materials are expressed in terms of the components of the principal stress directions, α, β and γ, as follows:

$$\begin{aligned}
&\varepsilon_\alpha - \theta_\alpha \Delta T = a_{11}\sigma_\alpha + a_{12}\sigma_\beta + a_{12}\sigma_\gamma \\
&\varepsilon_\beta - \theta_\alpha \Delta T = a_{12}\sigma_\alpha + a_{22}\sigma_\beta + a_{12}\sigma_\gamma \\
&\varepsilon_\gamma - \theta_\alpha \Delta T = a_{12}\sigma_\alpha + a_{12}\sigma_\beta + a_{13}\sigma_\gamma \\
&\varepsilon_{\alpha\beta} = \varepsilon_{\beta\gamma} = \varepsilon_{\gamma\alpha}
\end{aligned} \tag{3.13}$$

where diagonal elastic compliance a_{ii} and off-diagonal compliance $a_{ij}(i \neq j)$ are determined as:

$$\begin{aligned}
a_{ii} &= \frac{1}{E} \\
a_{ij} &= -\frac{\nu}{E}
\end{aligned} \tag{3.14}$$

The functionally graded material is implemented through continuous variation of elastic modulus along bond line which is governed by following linear function profile [165]:

$$f(I,s)_{T,C} = 1 + (R-1)\frac{s}{N(x,y,z)} \tag{3.15}$$

where s is the distance measured along the bond length, I is the hydrostatic stress and N is the ratio of length of bond and substrate.

$$
\begin{aligned}
&s = L(x), N(x) > N(y) \geq N(z) \\
&s = L(y), N(y) > N(x) \geq N(z) \\
&s = L(z), N(z) > N(y) \geq N(x) \\
&N(x,y,z) = \frac{L_s}{L_b} \\
&I = \frac{\sigma_{xx} + \sigma_{yy} + \sigma_{zz}}{3}
\end{aligned}
\tag{3.16}
$$

where L_s and L_b denote the length of substrate and length of bond, respectively and σ_{xx}, σ_{yy} and σ_{zz} are the normal stresses components of any stress tensor.

Material gradients are evaluated in terms of bimodular ratio (R) which is expressed as follow:

$$R = \left(\frac{E_2(I)}{E_1(I)} \right)_{T,C} \tag{3.17}$$

where $E_1(I)$ and $E_2(I)$ are the lower bound and upper bound Young Moduli of adhesive, respectively. T and C suffix used for the notation of tension and compression behavior under bimodularity.

The hydrostatic stress I is evaluated by using above equation. The modulus of elasticity for tension and compression depends on hydrostatic stress which is defined as a step function, explained as follows:

$$E_{1,2}(I) = \begin{cases} E_T(\,for + I) \\ E_C(\,for - I) \end{cases} \tag{3.18}$$

The modulus of elasticity for tension and compression is evaluated according the positive and negative values of hydrostatic stress and the iteration continues as the criteria define above to calculate the bimodulus ratio.

According to the symmetric nature of the compliance, off-diagonal compliance a_{ij} in terms of tensile and compressive modulus of elasticity can be defined as

$$a_{12} = a_{23} = a_{31} = -\frac{\nu_T}{E_T} = -\frac{\nu_C}{E_C} \tag{3.19}$$

where ν_T and ν_C are the Poisson's ratio for tension and compression, respectively.

It is assumed that a_{ij} is constant for tensile and compressive modulus of elasticity and not affected by the sign of stress. The assumptions of neglecting transverse normal stress and transverse shear deformation cannot be considered for moderately thick plate. However the analysis of plates with arbitrary profile becomes very complicated, so the derivation is restricted to the cylindrical bending of a flat plate. The effect of transverse normal stress on the deformation of the plate is generally smaller than that of transverse shear, so the former can be ignored in comparison to the latter.

Figure 3.4 shows a rectangular coordinate system x, y and z, is setup as y, parallel to the generator of a plate; z, perpendicular to the plane of a plate. Also thermal load is applied on plate. Equation (3.13) is transformed into the equations for cylindrical bending with respect to x, y and z coordinate system as follows:

$$\begin{aligned}
&\varepsilon_x - \theta_\alpha \Delta T = a_{11}\sigma_x + a_{12}\sigma_y + (a_{33} - a_{11})n_1^2\sigma_\gamma \\
&0 = a_{22}\sigma_y + a_{12}\sigma_x + \theta_\alpha \Delta T \\
&\varepsilon_z - \theta_\alpha \Delta T = a_{12}(\sigma_x + \sigma_y) + (a_{33} - a_{11})(1 - n_1^2)\sigma_\gamma \\
&\varepsilon_{xz} = (a_{11} + a_{33} - 2a_{12})\tau_{xz}
\end{aligned} \tag{3.20}$$

where n_1 stands for a cosine of an angle between γ and x axes.

The last equation in Equation (3.20) is expressed under the assumption that a similar relation of the conventional elastic material between the shearing stress and strain would

hold in an approximate manner because of the secondary nature of the transverse shear deformation effect on the total deformation when compared with that of in-plane stresses. Since the 'y' direction corresponds to one of the principal directions from a geometrical consideration, it can be indicated as parallel to the 'β' direction.

Principal directions in the xz plane are denoted by α and γ, respectively. As the transverse normal stress σ_z is neglected, principal stresses in xz plane can be expressed as

$$\left.\begin{matrix}\sigma_1\\ \sigma_2\end{matrix}\right\} = \frac{1}{2}\left\{\sigma_x \pm (\sigma_x^2 + 4\tau_{xz}^2)^{1/2}\right\} \tag{3.21}$$

This implies that

$\sigma_1 \geq 0$ and $\sigma_2 \leq 0$

So, either

$\sigma_1 = \sigma_\alpha, \sigma_2 = \sigma_\gamma$ or $\sigma_1 = \sigma_\gamma, \sigma_2 = \sigma_\alpha$

From the above equation it can be concluded that the sum of a_{11} and a_{33} becomes constant. Moreover, by considering Equation (3.19), the coefficient $a_{11} + a_{33} - 2a_{12}$ (in Equation (3.20)) behaves as constant and is not affected by the sign of any stress.

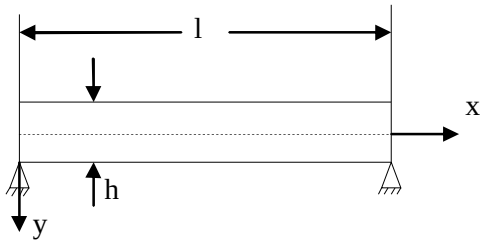

(a)

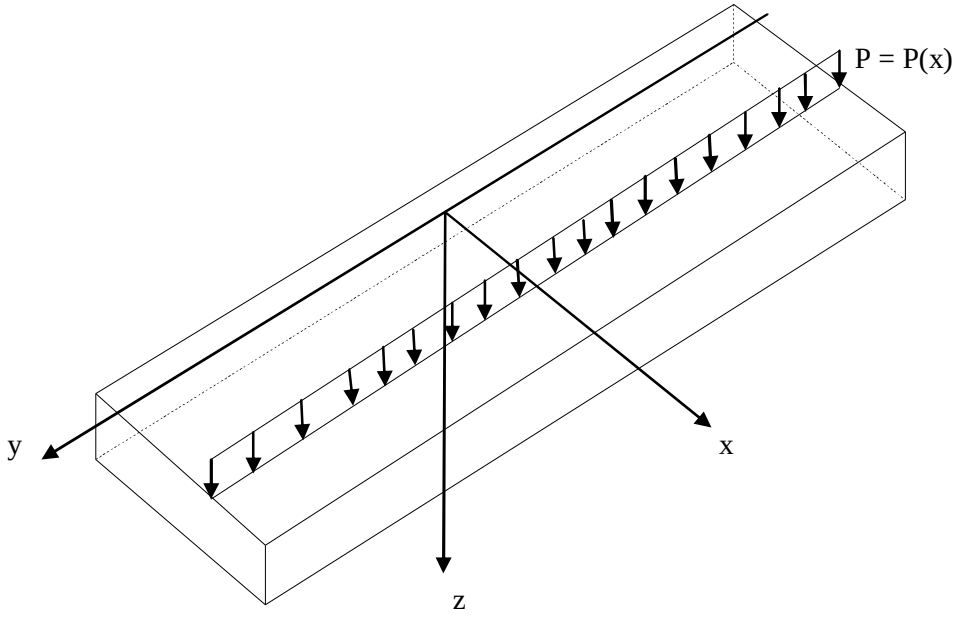

(b)

Figure 3.4 Rectangular plate (a) Loading condition (b) Coordinate system

A method from Ambartsumyan [9] for anisotropic plates or shells in consideration of the effect of the transverse shear can be applied. For the material which satisfies the relation $\frac{\nu_T}{E_T} = \frac{\nu_C}{E_C}$, the anisotropic material model reduces to that of Ambartsumyan's bimodular isotropic material model. Then, the functions, $f(z), X_1(x)$ and $X_2(x)$ are

introduced, where $f(z)$ is a function of coordinate of the thickness direction 'z' and vanishes on both surfaces of the plate $f(\pm h/2)=0$ and $X_1(x)$ and $X_2(x)$ are the functions of the coordinate in the x direction. Now τ_{xz} can be expressed as follows to satisfy boundary conditions on both sides:

$$\tau_{xz} = X_1(x) + X_2(x)\frac{z}{h} + f(z)\varphi(x) \tag{3.22}$$

where φ(x) is shear force

A lateral deflection and in-plane displacement in x direction is denoted as w and $u(x,z)$, respectively and transverse shear strain ε_{xz} is expressed as follows:

$$\varepsilon_{xz} = \frac{\partial u}{\partial z} + \frac{\partial w}{\partial x} \tag{3.23}$$

Substituting Eqs (3.22) and (3.23) into Equation (3.20), we obtained

$$\frac{\partial u}{\partial z} = (a_{11} + a_{33} - 2a_{12})\left\{ X_1(x) + X_2(x)\frac{z}{h} + f(x)\varphi(x) \right\} - \frac{\partial w}{\partial x} \tag{3.24}$$

It is supposed that the lateral displacement w is a function of x only i.e. $w = w(x)$ and does not vary in thickness direction z. Now considering $a_{11} + a_{33} - 2a_{12}$ as constant and then integrating w.r.t to z, the above equation becomes

$$u = (a_{11} + a_{33} - 2a_{12})\left\{ X_1(x)z + X_2(x)\frac{z^2}{2h} + \varphi(x)\int_0^z f(z)dz \right\} - z\frac{dw}{dx} + u_0(x) \tag{3.25}$$

where $u_0(x)$ stands for the magnitude of u at the middle plane of the plate that is at $z=0$, which implies $u_0(x) = u(x,0)$.

From Equation (3.25), ε_x is formulated as

$$\varepsilon_x = \frac{\partial u}{\partial x} = (a_{11} + a_{33} - 2a_{12}) \left\{ \frac{dX_1}{dx} z + \frac{dX_2}{dx} \frac{z^2}{2h} + \frac{d\varphi}{dx} \int_0^z f(z) dz \right\} - z \frac{d^2 w}{dx^2} + \frac{du_0}{dx} \tag{3.26}$$

In Equation (3.26), the last two terms in the right hand side are the same as for the expression based on conventional plate theory of Kirchhoff-Love, and then the first term of Equation (3.26) and the expression of ε_{xz} corresponds to a correction to the elementary theory of a bimodulus plate. If $f(z)$ is indicated by an appropriate function, the in-plane displacement and strain components can be expressed in concrete form.

From Equation (3.20), we obtained

$$\sigma_x = \frac{\varepsilon_x + \varepsilon_z - 2\theta_\alpha \Delta T + \frac{2a_{12}}{a_{22}} \theta_\alpha \Delta T + (a_{33} - a_{11}) \sigma_\gamma}{\left(a_{12} + a_{11} - \frac{2a_{12}^2}{a_{22}} \right)} \tag{3.27}$$

Also,

$$\sigma_y = -\frac{a_{12}}{a_{22}} \sigma_x = -\frac{a_{12}}{a_{22}} \left[\frac{\varepsilon_x + \varepsilon_z - 2\theta_\alpha \Delta T + \frac{2a_{12}}{a_{22}} \theta_\alpha \Delta T + (a_{33} - a_{11}) \sigma_\gamma}{\left(a_{12} + a_{11} - \frac{2a_{12}^2}{a_{22}} \right)} \right] \tag{3.28}$$

Using the stress-strain relation, we obtained

$$\sigma_z = \frac{E}{(1+\nu)(1-2\nu)} \left[\frac{1}{\left(a_{12} + a_{11} - \frac{2a_{12}^2}{a_{22}} \right)} \left\{ \begin{array}{l} \left(2\nu a_{12} + 2\nu a_{11} - \frac{4\nu a_{12}^2}{a_{22}} \right) \varepsilon_x + \left(\begin{array}{l} a_{12} - \nu a_{12} - \nu a_{11} + \\ a_{11} - \frac{2a_{12}^2}{a_{22}} + 2\nu a_{12}^2 \end{array} \right) \varepsilon_z + (2(\nu-1)a_{12} + 2(\nu-1)a_{11} - 4\nu a_{12}^2 + 2(1-\nu) + 2(3-\nu)\frac{a_{12}^2}{a_{22}} + 2(1-\nu)\frac{a_{11}a_{12}}{a_{22}} + \\ (2\nu-1)\frac{a_{12}}{a_{22}} + 4\left(\nu - \frac{a_{12}}{a_{22}} \right) a_{12}^3 \theta_\alpha \Delta T + (a_{33} - a_{11}) \left(1 - \nu + a_{12} - \nu a_{12} - \nu a_{11} + a_{11} - \frac{2a_{12}^2}{a_{22}} + 2\nu a_{12}^2 \right) \sigma_\gamma \end{array} \right\} \right] - \tag{3.29}$$

$$\frac{E}{1-2\nu} \theta_\alpha \Delta T$$

Using Equation (3.13) and the invariance identity of a summation of three principal strains, we find

$$\sigma_\gamma = \frac{\{(a_{11}a_{12} + a_{12}a_{22} - 2a_{12}^2)\varepsilon_\gamma + (a_{12}^2 - a_{12}a_{22})(\varepsilon_x + \varepsilon_z)\}}{\{a_{11}a_{22}a_{33} + 2a_{12}^3 - a_{12}^2(a_{11} + a_{22} + a_{33})\}} \tag{3.30}$$

3.4 Finite element formulation for generalized thermoelasticity

In this section, the governing equations of generalized thermoelasticity (the G–L theory) are summarized, followed by the corresponding finite element equations. The G–L theory of generalized thermoelasticity consists of the equilibrium equation

$$\sigma_{ij,j} + \rho f_i = \rho \ddot{u}_i \tag{3.31}$$

the heat transfer equation

$$\rho T \dot{\eta} = -q_{i,i} + \rho h \tag{3.32}$$

and the Fourier's heat conduction law

$$q_i = -k_{i,j}\theta_{,j} \tag{3.33}$$

where $\sigma_{i,j}$ is the stress, f_i is the body force, ρ is the mass density, u_i is the displacement, η is the entropy density, q_i is the heat flux, h is the heat source density, k_{ij} is the thermal conductivity coefficient, and $T = T_0 + \theta$ is the absolute temperature with θ and T_0 denoting the temperature changed and the reference temperature, respectively. In Equations (3.31)–(3.33), super-dot refers to the derivative with respect to time; comma followed by sub-index denotes the corresponding partial differentiation, and summation convention over repeated sub-indices applies.

Since only linear behavior is considered in this paper, the following linear constitutive equations are adopted, i.e.,

$$\begin{aligned} \sigma_{ij} &= C_{ijkl}\varepsilon_{kl} - \beta_{ij}(\theta + \tau_1\dot{\theta}) \\ \rho\eta &= \beta_{ij}\varepsilon_{ij} + c_E(\theta + \tau_2\dot{\theta}) \end{aligned} \tag{3.34}$$

where C_{ijkl} is the elastic stiffness,

$\varepsilon_{ij} = (u_{i,j} + u_{j,i})/2$ is the strain, β_{ij} is the thermal constant, and c_E is the specific heat capacity. It is noted that the G–L theory differs from the classical theory of thermoelasticity in that two relaxation time parameters τ_1 and τ_2 are involved in the constitutive equations (3.34). When τ_1 and τ_2 vanish identically, the G–L theory reduces to the classical thermoelasticity.

It should be noted that appropriate boundary conditions associated with the governing Equations (3.31)–(3.33) must be adopted in order to properly formulate a problem. When the displacement and temperature are prescribed on the surfaces A_u and A_θ, respectively, one has

$$u_i = \bar{u}_i \text{ on } A_u \text{ and } \theta = \bar{\theta} \text{ on } A_\theta \tag{3.35}$$

where $\bar{u}_i$ and $\bar{\theta}$ are the prescribed values. On the other hand, if surface traction and surface flux are applied to the corresponding surfaces A_σ and A_q, the following boundary conditions must be satisfied,

$$T_i = \sigma_{ji} n_j = \bar{T}_i \text{ on } A_\sigma \text{ and } Q = q_i n_i = \bar{Q} \text{ on } A_q \tag{3.36}$$

where $\bar{T}_i$ and $\bar{Q}$ are the given surface traction and flux, respectively.

The finite element equations of a generalized thermoelasticity problem can be readily obtained by following the standard procedure (Prevost and Tao (1983)). In the finite element method, the displacement component $\{u\}$ and temperature θ are related to the corresponding nodal values $\left\{u^{(e)}\right\}$ and $\left\{\theta^{(e)}\right\}$ by

$$\{u\} = [N]_{p\times n}\left\{u^{(e)}\right\} \qquad \theta = [N']_{t\times n}\left\{\theta^{(e)}\right\} \tag{3.37}$$

where $p = 2$ for the two-dimensional problems considered here, n is the number of nodes per element, and $[N]$ and $[N']$ are the shape functions for the displacement and temperature, respectively. With Equation (3.37), the strain $\{\varepsilon\}$ and temperature gradient $\theta_i' = \theta_{,i}$ can be expressed in terms of the nodal quantities $\left\{u^{(e)}\right\}$ and $\left\{\theta^{(e)}\right\}$ as

$$\{\varepsilon\} = [B]\left\{u^{(e)}\right\} \qquad \theta' = [B']\left\{\theta^{(e)}\right\} \tag{3.38}$$

The principle of virtual work for the generalized thermoelasticity is

$$\int_V \left[\delta\{\varepsilon\}^T\{\sigma\} + \delta\theta' q - \delta\theta\rho T_0\dot{\eta}\right]dV = \int_V \delta\{u\}^T\left(\rho\{f\} - \rho\{\ddot{u}\}\right)dV + \int_{A_\sigma} \delta\{u\}^T\{\bar{T}\}dA + \int_{A_q}\delta\theta\bar{Q}dA \tag{3.39}$$

Substituting the constitutive relations (3.34) and Equation (3.38) and neglecting the body force (the body force is not considered here), the finite element equations corresponding to Equations (3.31)–(3.33), (3.35) and (3.36) can be obtained as

$$\sum_{e=1}^{ne}\left(\begin{bmatrix} M_{11}^{(e)} & 0 \\ 0 & M_{22}^{(e)}\end{bmatrix}\begin{Bmatrix}\ddot{u}^{(e)}\\ \ddot{\theta}^{(e)}\end{Bmatrix} + \begin{bmatrix} 0 & -C_{12}^{(e)} \\ C_{21}^{(e)} & C_{22}^{(e)}\end{bmatrix}\begin{Bmatrix}\dot{u}^{(e)}\\ \dot{\theta}^{(e)}\end{Bmatrix} + \begin{bmatrix} K_{11}^{(e)} & -K_{12}^{(e)} \\ 0 & K_{22}^{(e)}\end{bmatrix}\begin{Bmatrix}u^{(e)}\\ \theta^{(e)}\end{Bmatrix} = \begin{Bmatrix} F_1^{(e)}\\ -F_2^{(e)}\end{Bmatrix}\right) \tag{3.40}$$

where ne is the total number of elements. The coefficients in Equation (3.40) and the right hand force vectors $\left\{F_1^{(e)}\right\}$ and $\left\{F_2^{(e)}\right\}$ are given below.

$$\left[M_{11}^{(e)}\right] = \int_{V^{(e)}} \rho[N]^T[N]dV \qquad \left[M_{22}^{(e)}\right] = \tau_2\int_{V^{(e)}} c_E\rho[N']^T[N']dV$$

$$\left[C_{12}^{(e)}\right] = \tau_1\int_{V^{(e)}}[B]^T[\beta][N']dV \qquad \left[C_{21}^{(e)}\right] = T_0\int_{V^{(e)}}[N']^T[\beta][B']dV$$

$$\left[C_{22}^{(e)}\right] = \int_{V^{(e)}} c_E T_0 \left[N'\right]^T \left[N'\right] dV \qquad \left[K_{11}^{(e)}\right] = \int_{V^{(e)}} \left[B\right]^T \left[C\right]\left[B\right] dV \tag{3.41}$$

$$\left[K_{12}^{(e)}\right] = \int_{V^{(e)}} \left[B\right]^T \left[\beta\right]\left[N'\right] dV \qquad \left[K_{22}^{(e)}\right] = \int_{V^{(e)}} \left[B'\right]^T \left[k\right]\left[B'\right] dV$$

$$\left\{F_1^{(e)}\right\} = \int_{A_\sigma} \left[N\right]^T \left\{\bar{T}\right\} dA \qquad \left\{F_2^{(e)}\right\} = \int_{A_\theta} \left[N'\right]^T \bar{Q} dA$$

3.5 Computation of energy release rate

Linear Elastic Fracture Mechanics (LEFM) is useful in describing the growth of delamination in composite laminates [74]. In fracture mechanics, the total strain energy release rate (SERR), G_T, is calculated along the delamination front and is consists of three individual components. The first component, G_I, emerges due to interlaminar tension. The second component, G_{II}, emerges due to interlaminar sliding shear and the third component, G_{III}, arises due to interlaminar scissoring shear. These Energy Release Rate (ERR) components are then compared to interlaminar fracture toughness values to predict the delamination growth. The interlaminar fracture toughness values are computed experimentally under mixed mode loading, i.e, mode I and mode II loading [75-77]. Based on the concepts of LEFM, the Virtual Crack Closure Technique (VCCT) and Modified Crack Closure Integral (MCCI) methods have been applied to calculate all the modes of ERR.

3.5.1 Virtual Crack Closure Technique (VCCT)

The finite element codes have been used to simulate delamination growth by means of proper interfacial elements able to release pairs of nodes on the delamination front which satisfy the conditions based on Strain Energy release rate (SERR). The Strain Energy

release rate can be evaluated by the VCCT equation along the delamination front at each pair of nodes for suitable growth criteria i.e three fracture modes: mode I (opening mode), mode II (forward shear mode) and mode III (parallel shear mode) (Figure 3.5).

The commonly used linear form of the Power Law Growth Criterion to check fail release [166] is given by,

$$f = \frac{G_{equiv}}{G_{equivc}} = \frac{G_I}{G_{Ic}} + \frac{G_{II}}{G_{IIc}} + \frac{G_{III}}{G_{IIIc}} \geq 1 \tag{3.42}$$

where G_i is the energy release rate associated to the fracture mode i and G_{ic} is the critical value of the energy release rate associated to the fracture mode i. The VCCT equation for elements with only corner nodes can be written as:

$$G_i = \frac{F_i \Delta u_i}{2\Delta A} \text{ with } i = I, II, III \tag{3.43}$$

where F_i is the force at delamination tip for the fracture mode i, Δu_i is the opening displacement for the fracture mode i and ΔA is the crack surface created by the delamination opening.

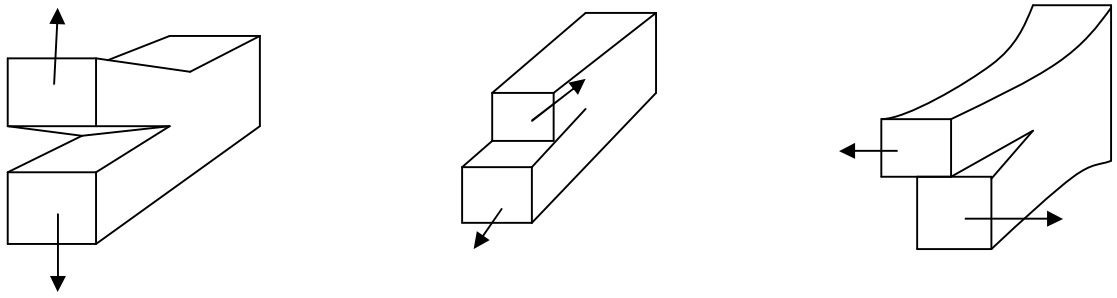

MODE I MODE II MODE III

Figure 3.5 Fracture modes

3.5.2 Modified Crack Closure Integral (MCCI)

Three dimensional finite element analysis is conducted to study the damage phenomena of composite laminates by the help of MCCI. The present study concerned with the analysis of thermo-elastic residual stress effect on the mixed-mode elliptical delamination crack growth behavior due to thermal and mechanical loading [78,79] (Figure 3.6). The figure shows the 8-noded element and this can be extended to 20-noded element. The advantage of 20-noded element over 8-noded is that 20-noded gives better results. A very fine mesh is necessary to obtain high quality results, and therefore high computer capacity.

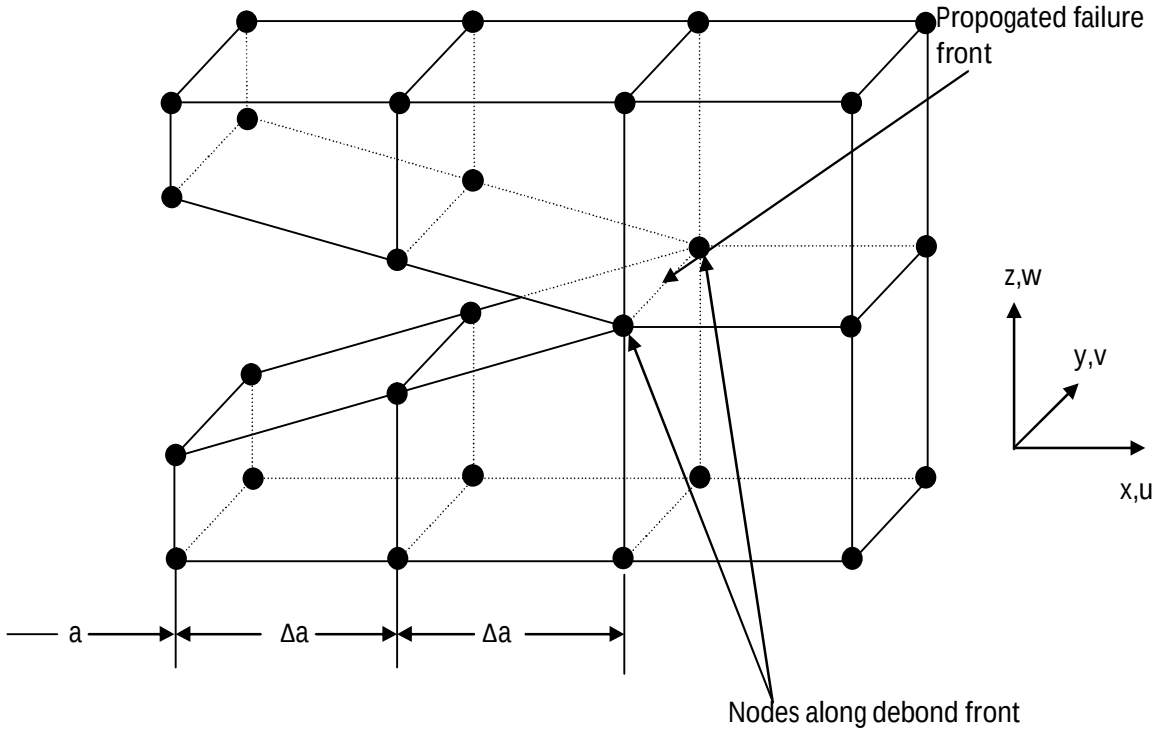

Figure 3.6 MCCI applied to the stiffened panel for computation of SERR

The strain energy release rate components at any point on the delamination front under mechanical and thermal loading due to uniform temperature drop from curing temperature to room temperature, is obtained by superposing their respective effects based on

assumptions of linear elasticity [80]. The energy released by the propagation of a crack of length a to $a+\Delta a$ can be expressed as [18],

$$W=\frac{1}{2}\int_{0}^{\Delta a}[\sigma_M(x)+\sigma_T(x)][\delta_M(x-\Delta a)+\delta_T(x-\Delta a)]dx \tag{3.44}$$

where the subscripts M and T represent mechanical and thermal loading respectively. $\delta(x-\Delta a)$ is the crack opening displacement between the upper and lower delaminated surfaces and $\sigma(x)$ is the stress at the crack front required to close the delaminated area. The three components of strain energy release rates for mode I, mode II and mode III can be expressed as follows.

$$\begin{aligned}
G_I &= \lim_{\Delta a\to 0}\frac{1}{2\Delta a}\int_{0}^{\Delta a}[\sigma_{zzM}(x)+\sigma_{zzT}(x)][\delta u_{zM}(x-\Delta a)+\delta u_{zT}(x-\Delta a)]dx \\
G_{II} &= \lim_{\Delta a\to 0}\frac{1}{2\Delta a}\int_{0}^{\Delta a}[\tau_{zxM}(x)+\tau_{zxT}(x)][\delta u_{xM}(x-\Delta a)+\delta u_{xT}(x-\Delta a)]dx \\
G_{III} &= \lim_{\Delta a\to 0}\frac{1}{2\Delta a}\int_{0}^{\Delta a}[\tau_{zyM}(x)+\tau_{zyT}(x)][\delta u_{yM}(x-\Delta a)+\delta u_{yT}(x-\Delta a)]dx
\end{aligned} \tag{3.45}$$

The total energy release rate G_T considering the thermal residual stress effects is the algebraic sum of the individual modes.

$$G_T = G_I + G_{II} + G_{III} \tag{3.46}$$

$[\sigma_{zz}\tau_{zx}\tau_{zy}]$ are the interlaminar stress. $\delta u_z, \delta u_x, \delta u_y$ are respectively the relative opening, sliding and tearing displacements of the initial delaminated surfaces to the final one along the delaminated interface.

For the superposition analysis, the stresses and displacements along the delamination front are calculated for the axial loading only without considering thermal residual stresses. Then

a separate analysis is performed, where the laminate is subjected to thermal loading only due to uniform temperature drop from the curing temperature. The stresses and displacements thus obtained are superposed with the results from uniaxial tensile loading for calculating the components of strain energy release rates due to the mechanical, thermal and superposition of these two loadings. The superposition procedure is followed as described above, the strain energy release rate around the delamination front is expressed in following equation. Substituting the values of individual components of strain energy release rate from Equation (3.45) in Equation (3.46), following expression for the total strain energy release rate G_T is obtained.

$$\begin{aligned} G_T &= G_I + G_{II} + G_{III} \\ &= \lim_{\Delta a \to 0} \frac{1}{2\Delta a} \int_0^{\Delta a} [\sigma_{zzM}(x) + \sigma_{zzT}(x)][\delta u_{zM}(x-\Delta a) + \delta u_{zT}(x-\Delta a)]dx \\ &+ \lim_{\Delta a \to 0} \frac{1}{2\Delta a} \int_0^{\Delta a} [\tau_{zxM}(x) + \tau_{zxT}(x)][\delta u_{xM}(x-\Delta a) + \delta u_{xT}(x-\Delta a)]dx \\ &+ \lim_{\Delta a \to 0} \frac{1}{2\Delta a} \int_0^{\Delta a} [\tau_{zyM}(x) + \tau_{zyT}(x)][\delta u_{yM}(x-\Delta a) + \delta u_{yT}(x-\Delta a)]dx \end{aligned} \tag{3.47}$$

Now rearranging and separating the terms with respect to individual parameters M, T and their interactions respectively in Equation (3.47), the expression derived has been stated next.

After reshuffling the similar subscripted terms, the expression for G_T is as follows.

$$
\begin{aligned}
G_T &= \underset{\Delta a\to 0}{Lim}\frac{1}{2\Delta a}\int_0^{\Delta a}[\{\sigma_{zzM}(x)\}\{\delta u_{zM}(x-\Delta a)\}+\{\tau_{zxM}(x)\}\{\delta u_{xM}(x-\Delta a)\}+\{\tau_{zyM}(x)\}\{\delta u_{yM}(x-\Delta a)\}]dx \\
&+\underset{\Delta a\to 0}{Lim}\frac{1}{2\Delta a}\int_0^{\Delta a}[\{\sigma_{zzM}(x)\}\{\delta u_{zT}(x-\Delta a)\}+\{\tau_{zxM}(x)\}\{\delta u_{xT}(x-\Delta a)\}+\{\tau_{zyM}(x)\}\{\delta u_{yT}(x-\Delta a)\}+ \\
&\{\sigma_{zzT}(x)\}\{\delta u_{zM}(x-\Delta a)\}+\{\tau_{zxT}(x)\}\{\delta u_{xM}(x-\Delta a)\}+\{\tau_{zyT}(x)\}\{\delta u_{yM}(x-\Delta a)]dx \\
&+\underset{\Delta a\to 0}{Lim}\frac{1}{2\Delta a}\int_0^{\Delta a}[\{\sigma_{zzT}(x)\}\{\delta u_{zT}(x-\Delta a)\}+\{\tau_{zxT}(x)\}\{\delta u_{xT}(x-\Delta a)\}+\{\tau_{zyT}(x)\}\{\delta u_{yT}(x-\Delta a)\}]dx \\
&=G_M+G_{MT}+G_{TH}
\end{aligned}
\tag{3.48}
$$

where,

$$
\begin{aligned}
G_M &= \underset{\Delta a\to 0}{Lim}\frac{1}{2\Delta a}\int_0^{\Delta a}[\{\sigma_{zzM}(x)\}\{\delta u_{zM}(x-\Delta a)\}+\{\tau_{zxM}(x)\}\{\delta u_{xM}(x-\Delta a)\}+\{\tau_{zyM}(x)\}\{\delta u_{yM}(x-\Delta a)\}]dx \\
G_{MT} &= \underset{\Delta a\to 0}{Lim}\frac{1}{2\Delta a}\int_0^{\Delta a}[\{\sigma_{zzM}(x)\}\{\delta u_{zT}(x-\Delta a)\}+\{\tau_{zxM}(x)\}\{\delta u_{xT}(x-\Delta a)\}+\{\tau_{zyM}(x)\}\{\delta u_{yT}(x-\Delta a)\}+ \\
&\{\sigma_{zzT}(x)\}\{\delta u_{zM}(x-\Delta a)\}+\{\tau_{zxT}(x)\}\{\delta u_{xM}(x-\Delta a)\}+\{\tau_{zyT}(x)\}\{\delta u_{yM}(x-\Delta a)]dx \\
G_{TH} &= \underset{\Delta a\to 0}{Lim}\frac{1}{2\Delta a}\int_0^{\Delta a}[\{\sigma_{zzT}(x)\}\{\delta u_{zT}(x-\Delta a)\}+\{\tau_{zxT}(x)\}\{\delta u_{xT}(x-\Delta a)\}+\{\tau_{zyT}(x)\}\{\delta u_{yT}(x-\Delta a)\}]dx
\end{aligned}
\tag{3.49}
$$

where, G_M , G_{MT} , and G_{TH} are the strain energy release rate components due to mechanical, superposition of individual effects thermo-mechanical loading and only thermal loading respectively.

3.6 Analysis of shifting of neutral axis due to bimodularity

It has been well recognized that most materials, including concrete, ceramics, graphite, and some composites, exhibit different tensile and compressive strains even when the same stress is applied in tension or compression. This gives rise to different elastic moduli in tension and compression. This leads to the calculation of both the elastic modulus for tension (E_T) and compression (E_C). Structural materials exhibiting different stress-strain curves in compression and tension are termed as bimodulus materials. Not only anisotropic

and orthotropic materials such as composites, but also some traditional isotropic materials as ceramics, graphites may also have different moduli in tension and compression. In the case of bimodulus materials the constitutive matrix is a function of stress. Though the stress-strain relationship is actually curvilinear, but it is approximated as bilinear with different slopes (Figure 1.6). Hence the analysis of structures made up of bimodulus materials is more involved. As graphite components are used under multiaxial stress conditions, therefore evaluation and prediction of bimodulus ratio (E_T/E_C) is important for structural design of components. Awani *et al*. [167] has established the influence of bimodularity on the characteristic strength of graphite by conducting several experiments and proposed analytical models to characterize size dependence strength of such category of materials. Two basic material models viz. Ambartsumyan [168-170] are being most widely used for characterizing such bimodulus behavior. Ambartsumyan material model is based on the criterion of positive-negative signs of principal stress state at a point in a stressed body. This model has found its application mostly to isotropic materials having bimodulus characteristics. Bert material model is based on the criterion of positive-negative signs in the longitudinal strain of fibers in orthotropic materials, and hence has its significance in research for laminated composites.

The Young's modulus (E) value of a material is normally determined by the slope of the stress-strain curve at the origin for a standard specimen. However, when nonlinearity of stress-strain curve is observed even at origin, the standard procedure of evaluation of modulus for a 0.1% strain based on elasticity theory overestimates it considerably. In flexural tests, unequal modulus for tension and compression causes the slender specimen to experience a shift in the neutral axis. Hence the location of maximum bending stress in

tension and compression are also shifted away from the geometric symmetric axis. Therefore, displacements need to be expressed as functions of the ratio of moduli (E_T/E_C). As shown in Figure 3.7**,** in a three point bending flexure test, the neutral axis shifted to account for the mismatch in tension and compression moduli. The shift in geometric symmetric axis and hence from the closed form solution of theory of simple bending fractional shift in neutral axis can be expressed in terms of moduli ratio as follows.

$$\frac{h_T}{h} = \frac{1}{\left[1+\left(\frac{E_T}{E_C}\right)^{\frac{1}{2}}\right]} \tag{3.50}$$

where, h_C and h_T are fractional height of the beam in compression and tension respectively and h is the total height of the beam.

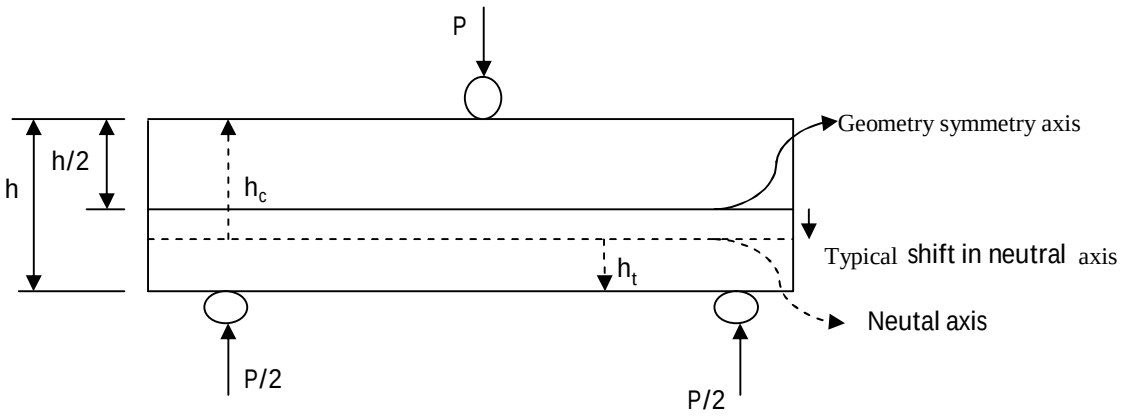

Figure 3.7 Schematic of three-point bending flexure specimen

Figure 3.8 shows a typical graphical representation of behavior of slender sections of bimodulus materials under flexure loading. This gives a typical nomenclature of percentage of beam in compression or tension with respect to variation of bimodulus ratio.

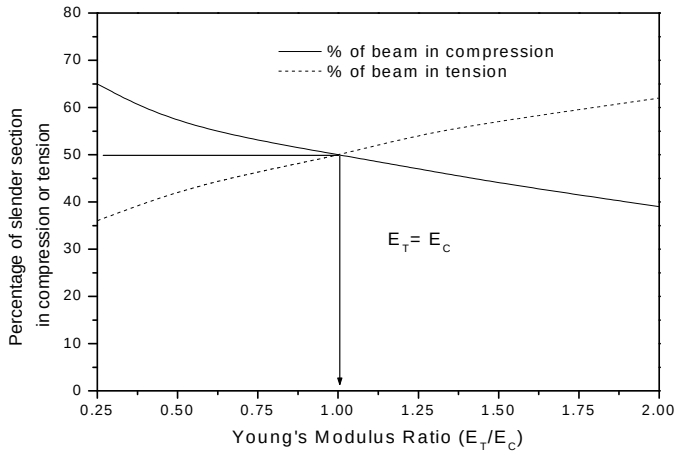

Figure 3.8 Typical schematic representation of percentage of beam in compression or tension with respect to bimodulus ratio of a slender flexure bimodulus specimen

The phenomena of different behavior in tension and compression were first recognized by Saint-Venant [171], however, the concept did not receive much attention for a long time from research community. Later on, the concept of a bimodulus material was originated by Timoshenko [172] while considering the flexural stress in such a material undergoing pure bending. The effective modulus for stiffness of such a beam in pure bending was given by Marin [173]. The bimodulus concept was extended to two-dimensional materials by Ambartsumyan [174]. Within the last few decades, several attempts have been made to establish constitutive relationships for such materials. Also, a lot of literature related to analytical and numerical solutions is available for the bending and shear deformation of bimodular beams. Though in the last few decades, some numerical analyses for the structural problems considering bimodulus behavior of the material have been done and the shifting of neutral axis in a complicated specimen of bimodular material but the more accurate reliability prediction remains really a challenging issue.

For the determination of shifting of neutral axis in bimodular specimen, three-point and four point bend tests have been performed in Comsol finite element based software. Stress analysis has been done on the specimen with graphite/epoxy material properties using finite element software. Figure 3.9 shows the normal stress distribution in x-direction for three point bend test and four point bend tests. The results reflect that the maximum value of stress in compression zone is quite high in comparison to tension zone, due to material bi-modularity. Young's Modulus of elasticity in tension (E_T) is quite high in comparison to compression (E_C) for graphite composite. Similar type of effect of bi-modularity is shown in von-Mises stress distribution (Figure 3.10). So the effect of bi-modularity is clearly visible in normal stress distribution in x-direction and von-Mises stress distribution.

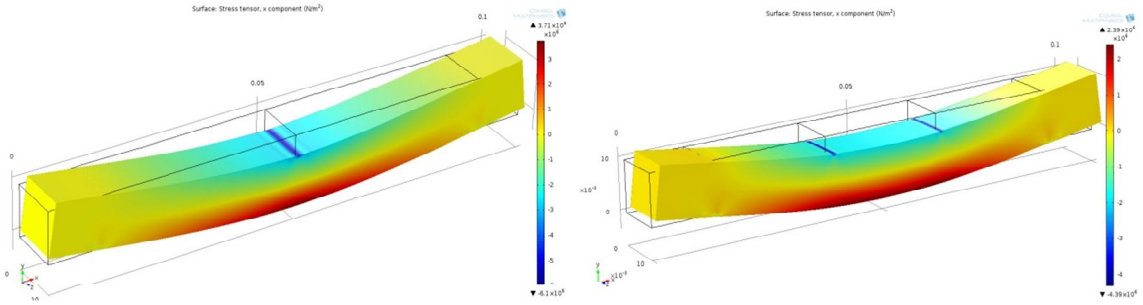

(a) (b)

Figure 3.9 Normal stress distribution in x- direction for (a) three point bend specimen and (b) four point bend specimen

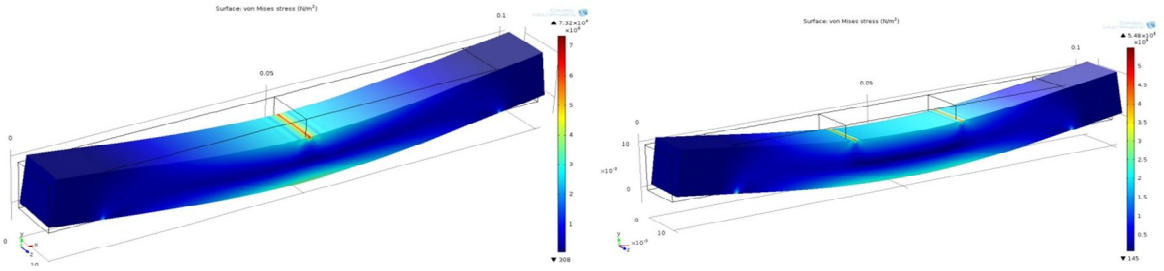

(a) (b)

Figure 3.10 von-Mises Stress distribution (a) three point bend specimen and (b) four point bend specimen

Figure 3.11 describes the variation of Young's modulus for the three-point and four-point flexure specimens indicating the asymmetric variation of tension and compression zone with respect to geometric centroidal axis. The tension zone is reflected by red color whereas compression is reflected by blue color in 3D geometry in three point and four point bend specimens shown in Figure 3.11. The tension and compression zones and shifting of neutral axis due to difference in modularity in tension and compression under three point loading condition is shown in Figure 3.12. The detailed data for shifting of neutral axis at vertical cross-section at various locations and analytically calculated neutral axis shift in three point bend specimen is represented in Table 3.1.

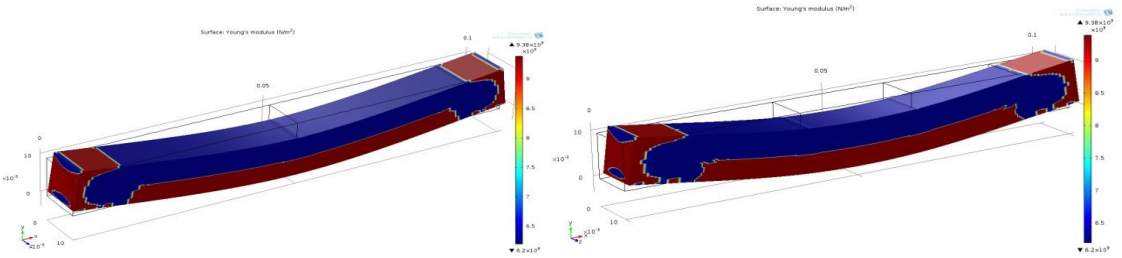

(a) (b)

Figure 3.11 Young's Modulus plot for (a) three point bend specimen and (b) four point bend specimen

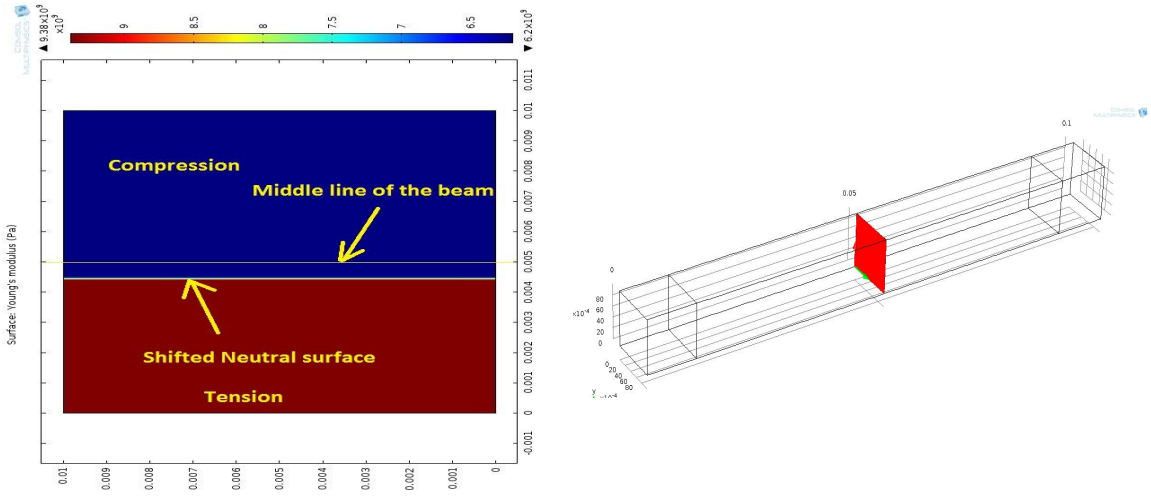

(a) (b)

Figure 3.12 (a) Young's Modulus plot on middle surface of the beam for three point bend specimen and (b) the plane at which the figure (a) is plotted

Table 3.1 The results obtained from the three point bend specimen simulation

E_T	9382.208 MPa
E_C	6198.801 MPa
Ratio	1.513
Neutral axis location	4.497 mm
Neutral axis shift at 50 mm	-0.502 mm
Analytical neutral axis location	4.483 mm
Analytical neutral axis shift	-0.516 mm

3.7 Conclusion

This chapter includes the theory and equations related to the objectives of the thesis. In the first section, the equations related to bimodularity and shifting of neutral axis due to the bimodular behavior have been included. Further, governing equations based on the functionally graded bimodularity under thermo-elasticity and finite element formulation for generalized thermoelasticity have been given. It has been well recognized that most materials, including concrete, ceramics, graphite, and some composites, exhibit different tensile and compressive strains even when the same stress is applied in tension or compression. This gives rise to different elastic moduli in tension and compression. As

composites are used under multiaxial stress conditions, therefore evaluation and prediction of modulus ratio is important for structural design of components. This leads to the calculation of both the elastic modulus for tension (E_t) and compression (E_c). Calculation of bimodulus ratio and shifting of neutral axis of graphite/epoxy composite has been done through FE based software.

Some conclusion has been summarized from the present work as follows.

1. The bimodular material exhibits two different stress-strain plots for tension and compression.

2. The bimodular behavior causes the neutral axis shifting on the application of flexural load and affects the state of stress under tensile and compressive loadings.

3. Maximum value of stress in compression zone is quite high in comparison to tension zone, due to material bi-modularity. Young's Modulus of elasticity in tension (E_T) is quite high in comparison to compression (E_C) for graphite composite.

Influence of bimodularity has been found to be predominantly affecting the state of stress of flexural specimens. The shift in neutral axis indicates the severity of tensile or compression regions with reference loading pattern in the numerical illustrations. Therefore in design of high risk structures, the uncertainty of failure modes needs to be revisited. It can be stated here that structures containing high stress gradient zones or stress raisers should be designed based on bimodular stress dependent elasticity concepts rather than unimodular constitutive procedures though the former involves significant complexity of incorporating elasticity as a function of stress state. In subsequent chapters endeavors has been made to characterize fracture behavior of adhesive bonded joints with consideration of bimodular interface behavior.